Chapter 7

High Pressure Studies on Materials Exhibiting the Fluid to Hexatic Phase Transition

High pressure studies on *fluid* to hexatic transition

7.1 Introduction

Application of high pressure adds a new dimension to investigate the rich variety of phases and phase transitions in liquid crystals. Some of the significant results obtained from such investigation are pressure-induced mesomorphism,[1,2] suppression of mesophases at high pressure,[3] re-entrant phases[4] etc. Pressure can alter not only the stability of the different phases, but can also change the nature of the transitions and they can have some important consequences. For example, it is well known that three first order lines meeting at a point results in a triple point.[2, 3,5] If one or more of the transitions are second order, a variety of critical points can occur, e.g., the tricritical point,[3,6] critical end point,[7] multicritical point[8,9] and all these have been observed in the pressure-temperature plane of single component systems. Other interesting observations include the recently discovered triply re-entrant behaviour at higher pressures.[10] Here we describe our studies on the effect of pressure on compounds exhibiting the fluid to hexatic transition.

As discussed in earlier chapters (see chapters 2 and 3) hexatic phases are characterised by three dimensional long range bond orientational order but with short range in-plane positional order. In hexatic B (hex B) the orientation of the molecules is along the layer normal whereas srnectic I (Sm I) and smectic F (Sm F) are tilted hexatics. In this chapter we present high pressure studies on materials exhibiting smectic A (Sm A)-hex B, Sm A-Sm F, smectic C (Sm C) - Sm I and Sm C-Sm F transitions.

High pressure studies on *fluid* to hexatic transition

7.2 Experimental

7.2.1 Materials Used

Experiments have been carried out on the following materials, viz.,

1. n-butyl 4'-n-hexyloxybiphenyl-4-carboxylate (46OBC)
2. (+)-(4-(2′-methylbutyl)phenyl 4′-n-octylbiphenyl-4-carboxylate) (8SI*)
3. N(4-n-nonyloxybenzylidine)-4-n-butylaniline (9O.4)
4. Terephthal-bis-octylaniline (TBOA)

The structural formulae and transition temperatures of these compounds are given Table 7.1.

7.2.2 High pressure set up

The experiments have been carried out using a calibrated high pressure optical cell that was available in our laboratory.[11] A brief description of this set up is given below.

High pressure optical cell

The schematic diagram of the high pressure optical cell is shown in figure 7.1. The main features of this cell are **(1)** it can be used for both light scattering studies and for optical microscopy experiments. The latter facility is needed

High pressure studies on fluid to *hexatic* transition

460 BC

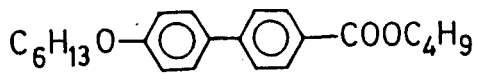

Isotropic $\xrightarrow{91.8}$ Sm A $\xrightarrow{65}$ Hex B

8SI*

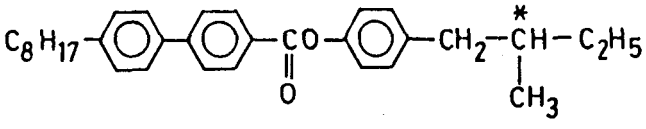

Isotropic $\xrightarrow{139.8}$ Blue phase $\xrightarrow{135.9}$ Cholesteric $\xrightarrow{134.1}$ Sm A $\xrightarrow{84.4}$ Sm C* $\xrightarrow{68.3}$ Sm I* $\xrightarrow{64.3}$ Sm F* $\xrightarrow{62.3}$ Cry G

90.4

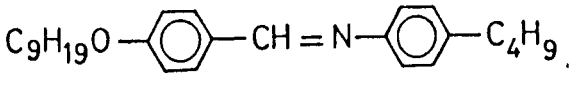

Isotropic $\xrightarrow{81.5}$ Sm A $\xrightarrow{68.8}$ Sm F $\xrightarrow{\sim 66.5}$ Cry G

TBOA

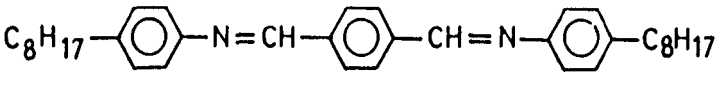

Isotropic $\xrightarrow{202.5}$ Sm A $\xrightarrow{192.5}$ Sm C $\xrightarrow{156.5}$ Sm F $\xrightarrow{137.0}$ Cry G

Table 7.1: Structural formulae and transition temperatures (in °C) of 46OBC, 8SI*, 90.4 & TBOA.

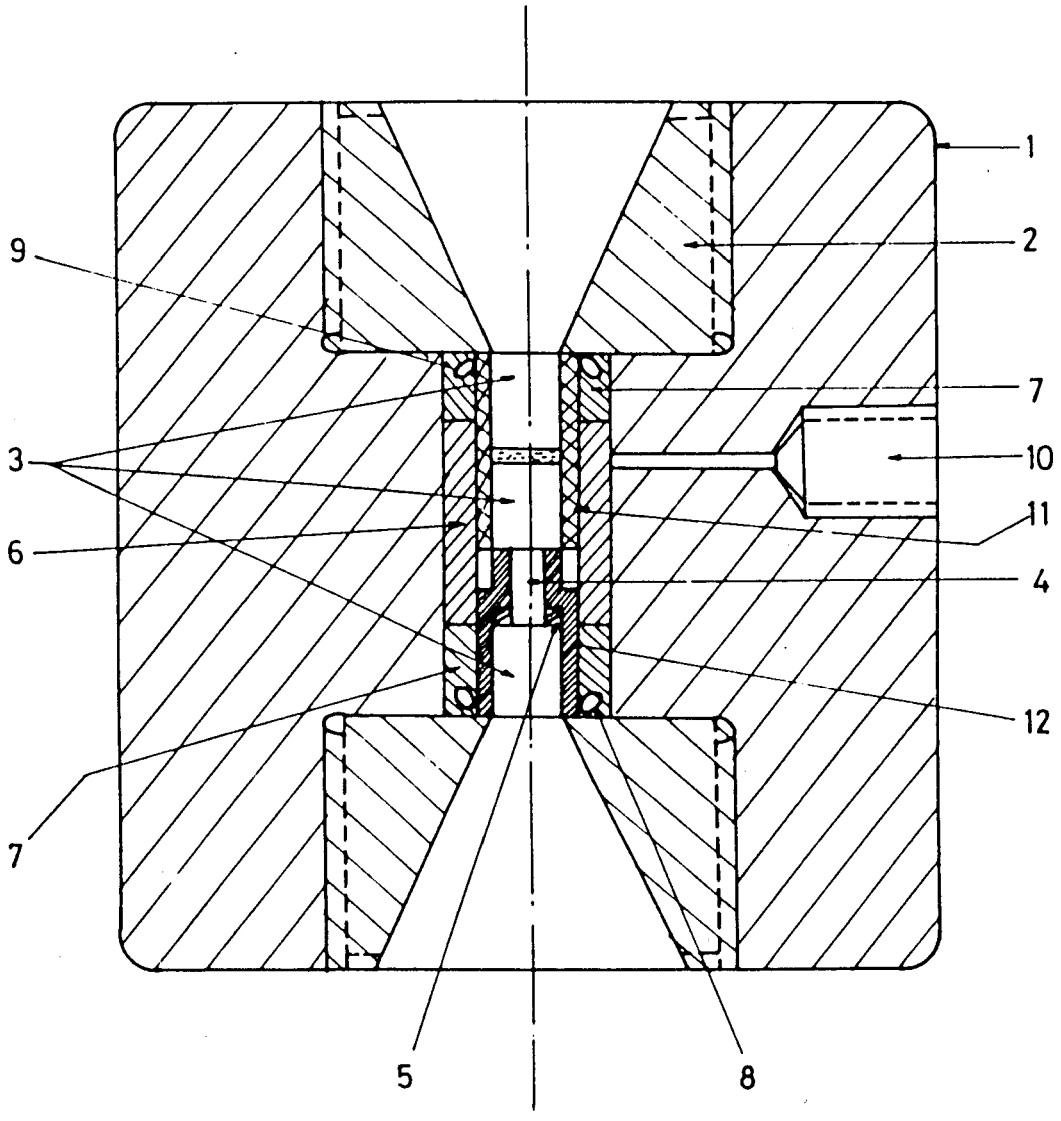

1. CELL BODY 2. STEEL PLUG 3. SAPPHIRE CYLINDERS
4. GLASS ROD 5. WASHER AND SPRING 6. CENTRE SPACER
7. OUTER SPACER 8. '0' RING 9. ANTIEXTRUSION RING
10. HIGH PRESSURE CONNECTION 11. FLURAN TUBE 12. LOW-PRESSURE SEALER

Figure 7.1: High pressure optical cell.

to identify any pressure induced phases. (2) It can be used with very small quantities ($\leq$ 5 mg) of the sample.

All the components of the cell are machined out of a low alloy hardenable steel, viz., **EN-24.** The body of the cell has threaded openings on both sides into which the two plugs with exactly matching threads can be fitted (see figure 7.1). On the outside the threads have large tapered openings (70^{o} outside taper) which facilitate a wide viewing angle without affecting the strength of the plug. On the inside, the plugs have small protrusions which are made optically flat by handlapping. These plugs keep the sample assembly in position. The central hole of the upper plug is sealed by an optically polished sapphire rod which also forms a part of the sample assembly. The hole in the cell body for the pressure connection consists of two stages: a smaller hole which extends from the interior of the body to about two-thirds of the thickness and joins a larger hole bored from outside.

To develop high pressure in the small central sample chamber it is essential to have tight sealing along both boundaries of the plugs; one for the central hole and the other along the circular boundary of the chamber against the plug. The thin clearance between the plug and the sample chamber caused by a slight lifting of the plug by high pressure leads to a leak of the oil to outside. This leak is avoided by placing around the junction a neoprene 'O' ring in conjunction with an anti-extrusion ring. The seal at the central hole of the plug is made with optically polished sapphire windows and a small washer made of thin aluminium foil. The sapphire windows as well as the 'O' ring are held in position initially

by the outer spacer.

Encapsulation of the sample

Figure 7.2 shows the schematic diagram of the sample assembly. The sample is sandwiched between two sapphire rods which fit snugly inside a fluran tube. Fluran is an elastomer material which does not react with liquid crystals and at the same time transmits the pressure exceedingly well. It can withstand temperatures upto 270°C. An effective sealing is realised by tightly wrapping a thin steel wire around the tubing on the sapphire windows. The inner spacer (low pressure sealer), washer and the spring (sec figure 7.1), centre the bottorn sapphire of the sample and keep it under high tension. The third sapphire which is completely isolated from the sample assembly seals the bottom end of the pressure cell. The space between this third sapphire and the bottom sapphire of the sample assembly is occupied by a glass rod thereby reducing the amount of oil between these two sapphires which otherwise would have reduced the intensity of the transmitted light. All the three sapphire rods are cut such that the C-axis is perpendicular to the faces.

The heating system is made of an aluminium cylinder whose internal diameter is such that the pressure cell could be push-fitted into it. Nichrome tape is wound on a mica sheet (which serves as an electric insulator) is in turn wrapped around the inside wall of the aluminium cylinder. Temperature of the sample is measured by using a calibrated chromel-alumel thermocouple placed close to the sample.

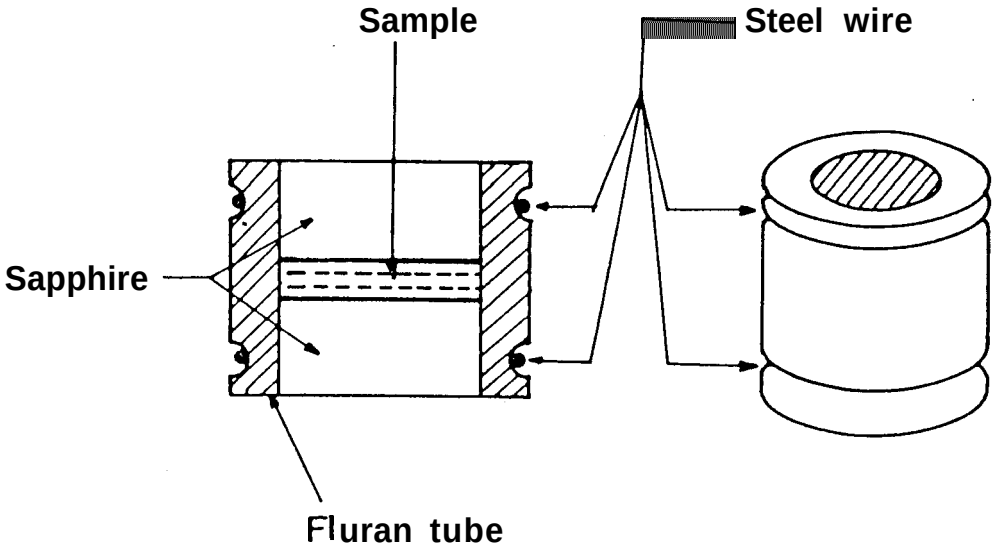

Figure 7.2: Sample assembly.

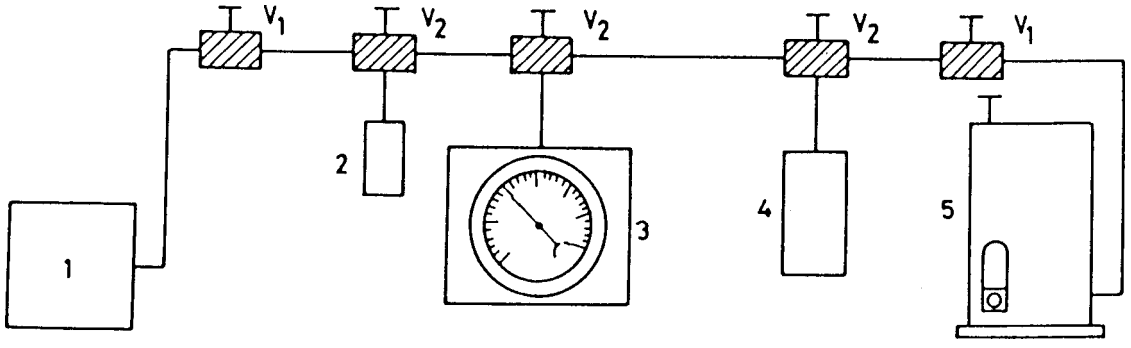

Figure 7.3: Schematic diagram of the high pressure plumbing system. (1) High pressure cell, (2) Pressure transducer, (3) Bourdon gauze, (4) Pressure generator, (5) Hand pump. $V_1 \rightarrow$ Two-way valve, $V_2 \rightarrow$ Three-way valve.

High pressure plumbing system

The schematic diagram of the high pressure plumbing system used in the present study is shown in the figure **7.3.** A hand pump (PPI, USA) is used to generate the pressure in the cell. Fine variation of the pressure is achieved by using a pressure generator (HIP, USA) with a small displacement capacity. The line pressure, which is nothing but the pressure experienced by the sample is measured by a Bourdon type (Heise) gauge. The plumbing connections are made through two-way arid three-way valves. The valves as well as the tubing were chosen to withstand line pressures up to 7 kbar.

The pressure is applied to the sample in a straightforward way. Pulling the handle of the hand pump raises the piston and draws oil from the reserve into the pump's chamber. Pushing the handle down lowers the piston which compresses the oil and sends it through the steel oil line to the cell. After this priming operation the pressure could be fine controlled using the pressure generator. As the pressure in the cell is same as that in the pump, the cell pressure could be directly measured by measuring the line pressure.

7.2.3 A typical experiment

The block diagram of the experimental setup used to determine the transition temperature is shown in figure **7.4.** Light from a He-Ne laser (Spectra Physics Model 120S) was made to fall on the sample in the optical cell. A photo detector (Model Motorola, MRD **360)** system was positioned to collect the light transmitted by the sample. The voltage drop across a fixed resistance of 1 kΩ

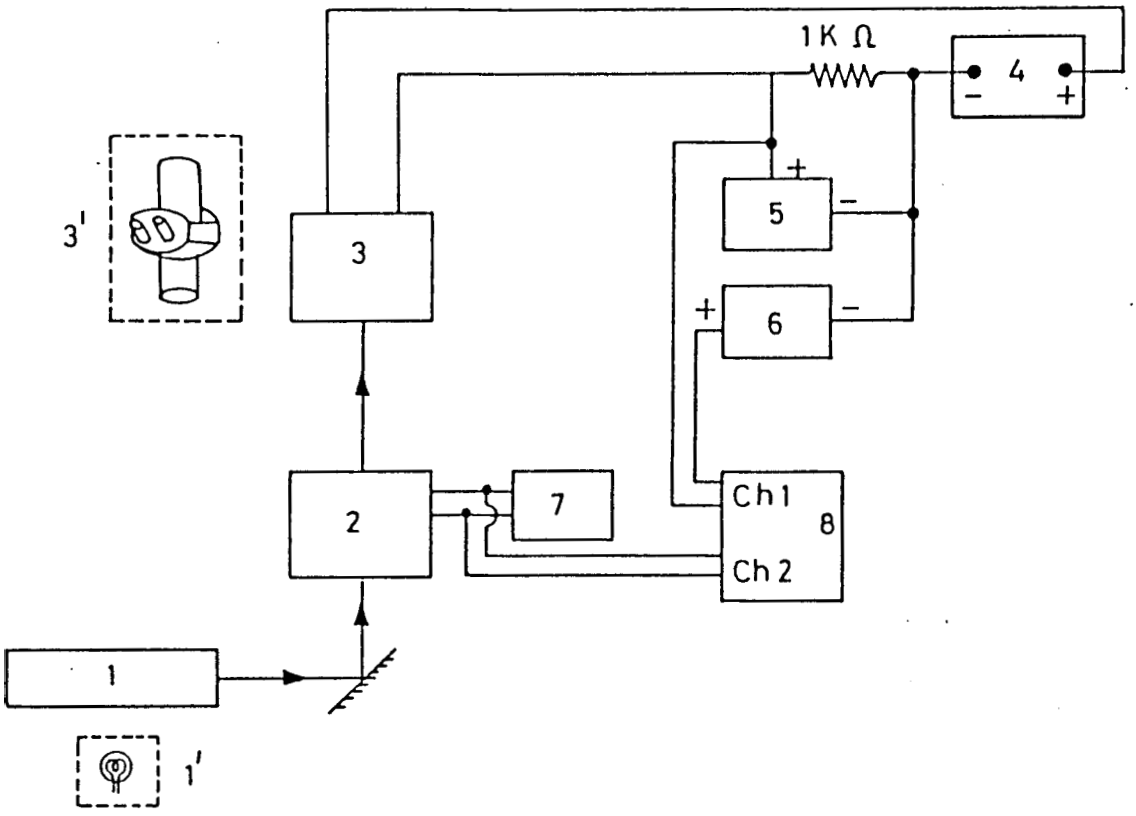

Figure 7.1: Schematic diagram of the experimental sot up used for the high pressure experiments. 1. He-Ne laser, 2. High pressure optical cell, 3. Photo-detector, 4. Photo-detector bias power supply, 5. Multirneter for measuring intensity in terms of voltage, 6. DC standard source used for voltage offset, 7. Multimeter for measuring thermocouple output, 8. Multichannel recorder. *Instruments* indicated *by primed numbers are used* for *microscopic* observations.

caused by the current output of the detector was measured using a digital multimeter (Keithley Model 174). A parallel connection from this was given to one of the channels of a multichannel recorder (Linseis model 2041). The temperature of the sample was measured using a thermocouple in conjunction with a programmable digital multimeter (Keithley 181). The voltage output of the thermocouple was fed to another channel of the multichannel recorder. Thus both intensity and temperature could be simultaneously monitored and recorded. At the phase transition there would be an abrupt change in the intensity of the transmitted light. The precision in measuring the pressure was ± 1.5 bar and the temperature $\pm 0.02^{o}$C.

7.3 Results and Discussion

7.3.1 46OBC (Sm A-hex B transition)

Figure 7.5 shows a pressure-temperature (P-T) phase diagram. Two interesting features of this diagram are (a) The temperature range of both smectic A and hexatic phases remains the same till the highest pressure studied (2.1 kbar). (b) The slopes dP/dT obtained being the same ($\sim 28\ bar/^{o}$C) for both isotropic-Sm A and Sm A-hex B phase boundaries (see Table 7.2) is comparable to that obtained for another compound (65OBC) showing Sm A-flex B transition.[12]

7.3.2 8SI* (Sm C*-Sm I' transition)

The P-T diagram of 8SI* is shown in the figure 7.6. The notable features of this diagram are

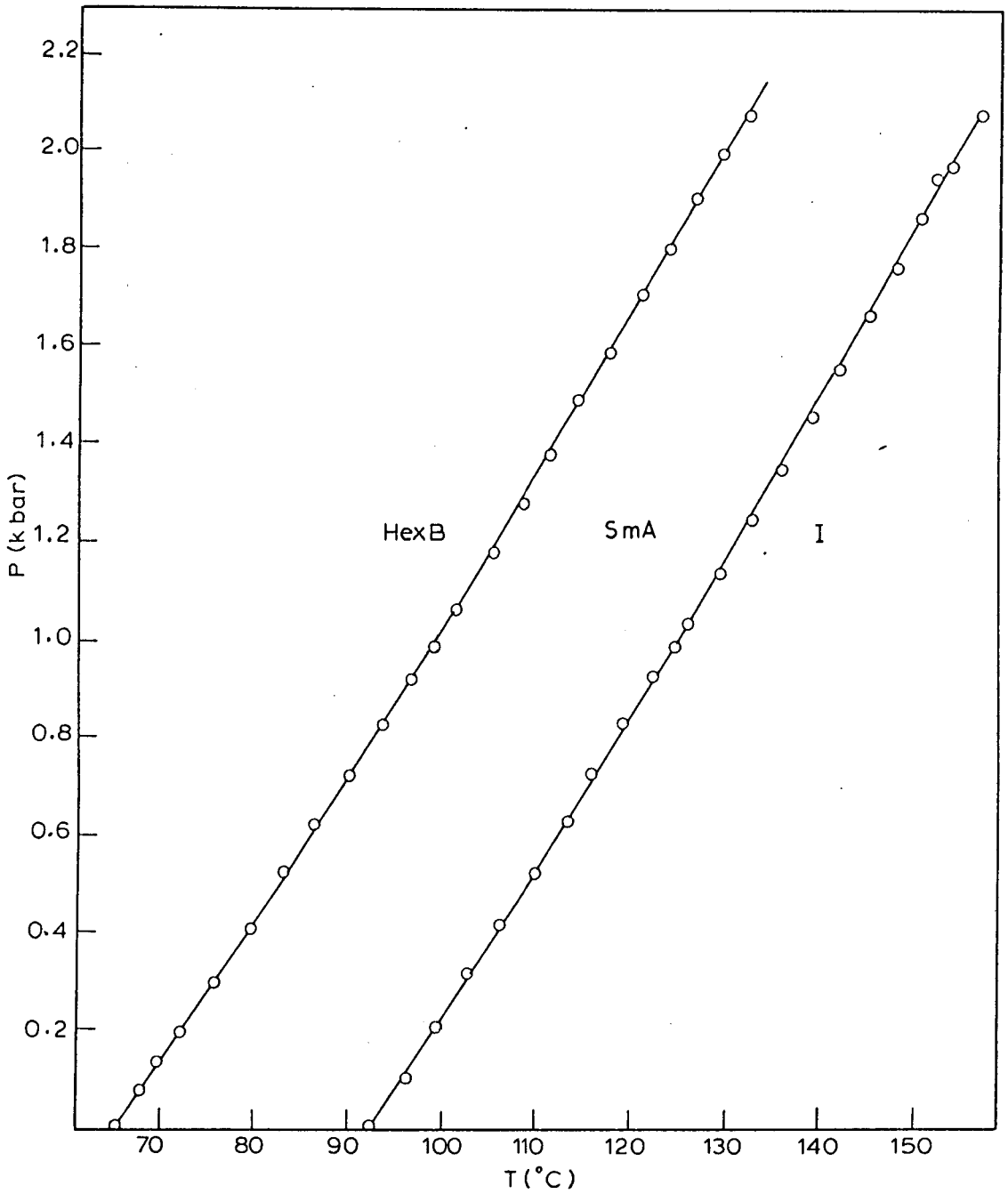

Figure 7.5: Pressure-temperature (P-T) diagram for 4OOBC. Isotropic-Sm A phase boundary is parallel to Sm A-hex B phase boundary.

High pressure studies on *fluid* to hexatic transition

Table *7.1:* $\left(\frac{dP}{dT}\right)_{\text{at 1 bar,}}$ values for 46OBC.

	Transition	$\frac{dP}{dT}$ bar / °C
1	Isotropic - Sm **A**	28.9
2	Sm A - hex B	27.7

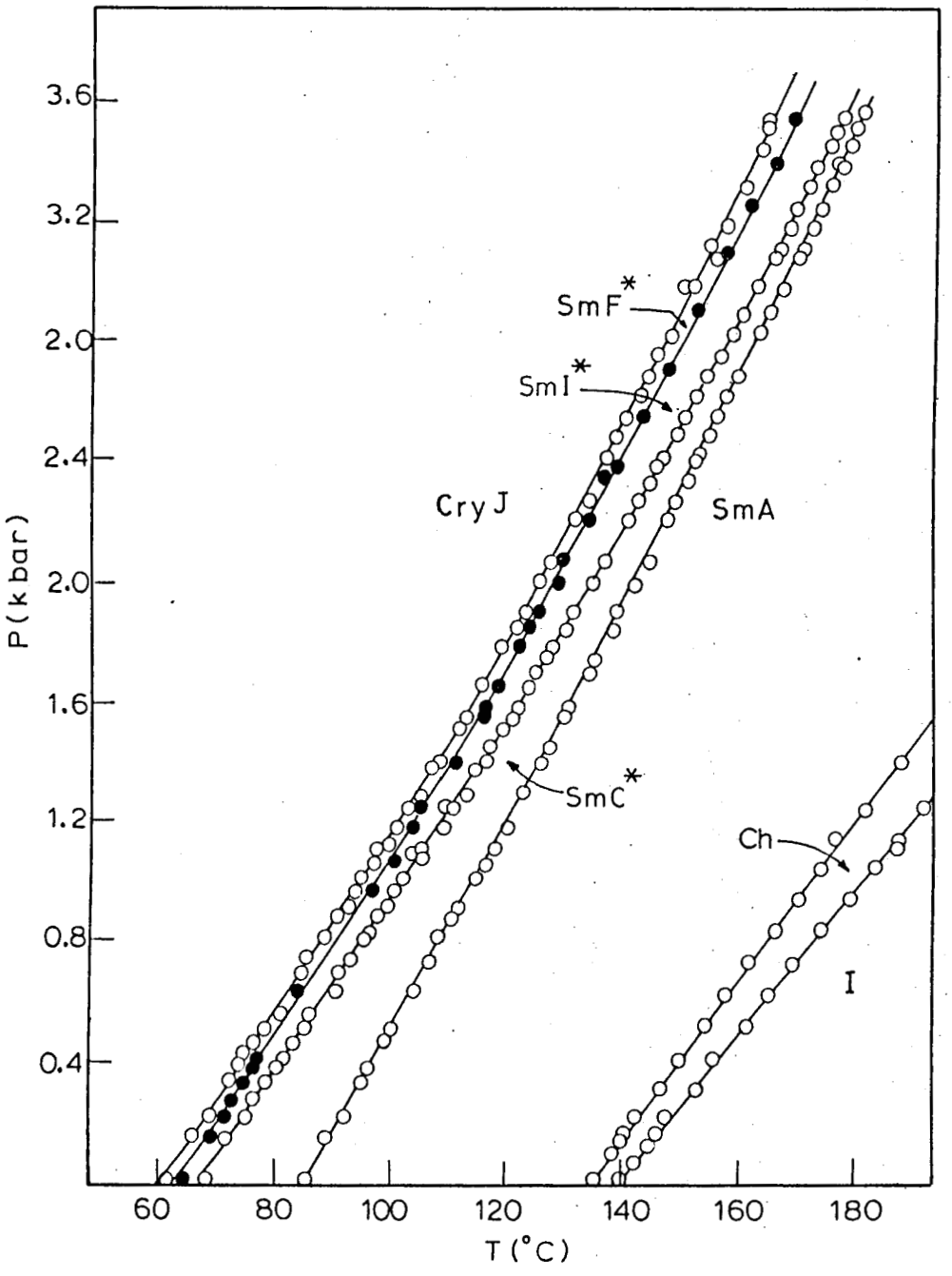

Figure 7.6: P-T diagram for 8SI*. For the sake of clarity Sm I*-Sm F* phase boundary is marked with filled circles. The decrease(increase) in the stability of Sm C*(Sm A & Sm I*) phase with pressure leads to a possible Sm A-Sm C*-Sm I* meeting point at $\sim$ 4.7 kbar.

1. The temperature range of the Sm A phase increases with increase in pressure. This is at the expense of the temperature range the Sm **C*** phase. Also the range of the Sm I* phase increases with increase in pressure. The destabilisation of the Sm **C*** phase under high pressure is a well known fact.[13] The reduction in the Sm C* range accompanied by an increase in the temperature range Sm **A** and Sm I* phases may result in a possible *Sm A-Sm C*-Sm I* meeting point* at higher pressures. Extrapolating our data it appears that such a point may occur at —4.7 kbar, a pressure which is beyond the limit of our set up.

2. The temperature range of the lower temperature hexatic phase, Sm F* remains unaltered by the application of pressure.

The dP/dT values at 1 bar for different phase boundaries are given in the Table **7.3.** Some of the features seen here have also been observed in 9OSI, a structurally similar material.[14]

7.3.3 90.4 (Sm A-Sm F transition)

P-T phase diagram is shown in the figure 7.7. A very significant result observed is the **Pressure induced mesomorphism.** This compound exhibits Sm **A**-Sm F-Cry G phase sequence at atmospheric pressure and continues to do so up to a pressure of —0.6 kbar. Beyond this pressure, the phenomena of pressure induced mesomorphism is observed; the Sm F phase does not go directly to the Cry G phase but through a new phase (hereafter referred to as 'X' phase). Microphotographs taken at 1.24 kbar showing optical textures observed in Sm **A,**

High pressure studies on fluid to hexatic transition

Table 7.3: $\left(\frac{dP}{dT}\right)_{at\ 1\ \text{bar}}$ values for 8SI*.

	Transition	$\frac{dP}{dT}$ bar / °C
1	Isotropic - Cholesteric	23.7
2	Cholesteric - Sm A	27
3	Sm A - Sm C*	34.6
4	Sm C* - Sm I*	29.1
5	Sm I* - Sm F*	29.3
6	Sm F* - Cry J	30

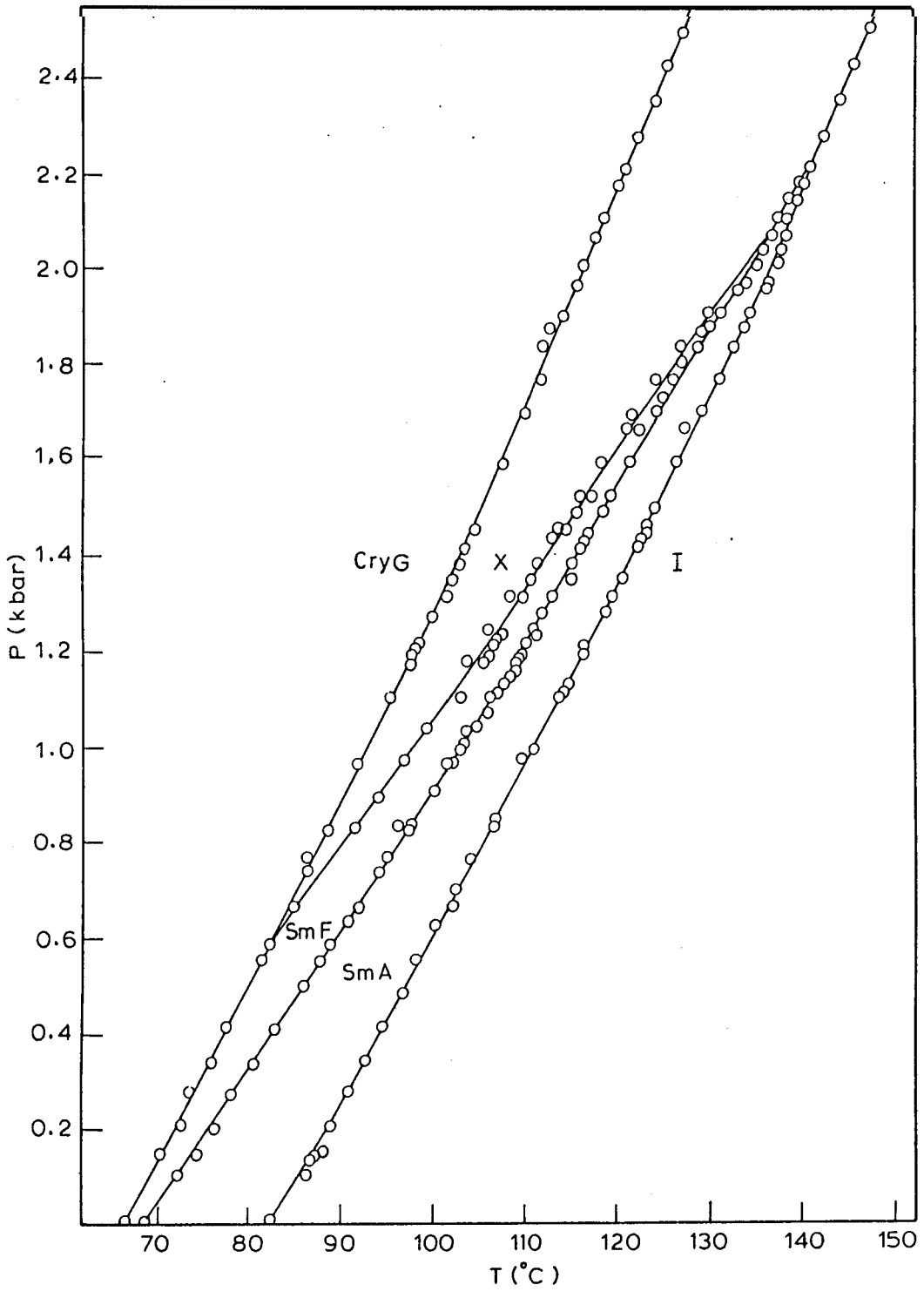

Figure 7.7: P-T diagram for 90.4. **A** new phase ('X') is induced above —0.6 kbar. There are two triple points viz., Sm A-Sm F- X and Isotropic-Sm A-X.

Sm F and the newly induced 'X' phase are given in figure 7.8. Raw scans of the intensity variation across the isotropic-Sm A, Sm A-Sm F, Sm F-Cry G transitions at 0.28 kbar are shown in figure 7.9a. Figure 7.9b is a run taken at a higher pressure (1.7 kbar). The appearance of the X phase between the Sm F and Cry G phases is clearly observed. Scan taken at a much higher pressure (2.5 kbar) shows only the isotropic-X-Cry G phase sequence (see figure 7.9c). The optical observation of the textures at higher pressure suggests that the X phase could be a higher order smectic phase. However, X ray studies at high pressure are needed to identify this phase.

The temperature range of both Sm A and Sm F phases decrease with increase in pressure and get suppressed at higher pressure resulting in two triple points, namely, Sm A-Sm F-Sm X and isotropic-Sm A-X. Whereas the range of newly induced phase 'X' increases with increase in pressure.

Table 7.4 gives dP/dT values for different phase boundaries for 90.4.

7.3.4 TBOA (Sm C-Sm F transition)

The pressure-temperature phase diagram is shown in the figure 7.10. It is observed that the Sm C phase temperature range decreases with increasing pressure. The dP/dT value for the Sm A-Srn C phase boundary is large compared to the Sm C-Sm F phase boundary. (see Table 7.5). In contrast, the Sm C - Sm F and Sm F-Cry G phase boundaries remain parallel to one another.

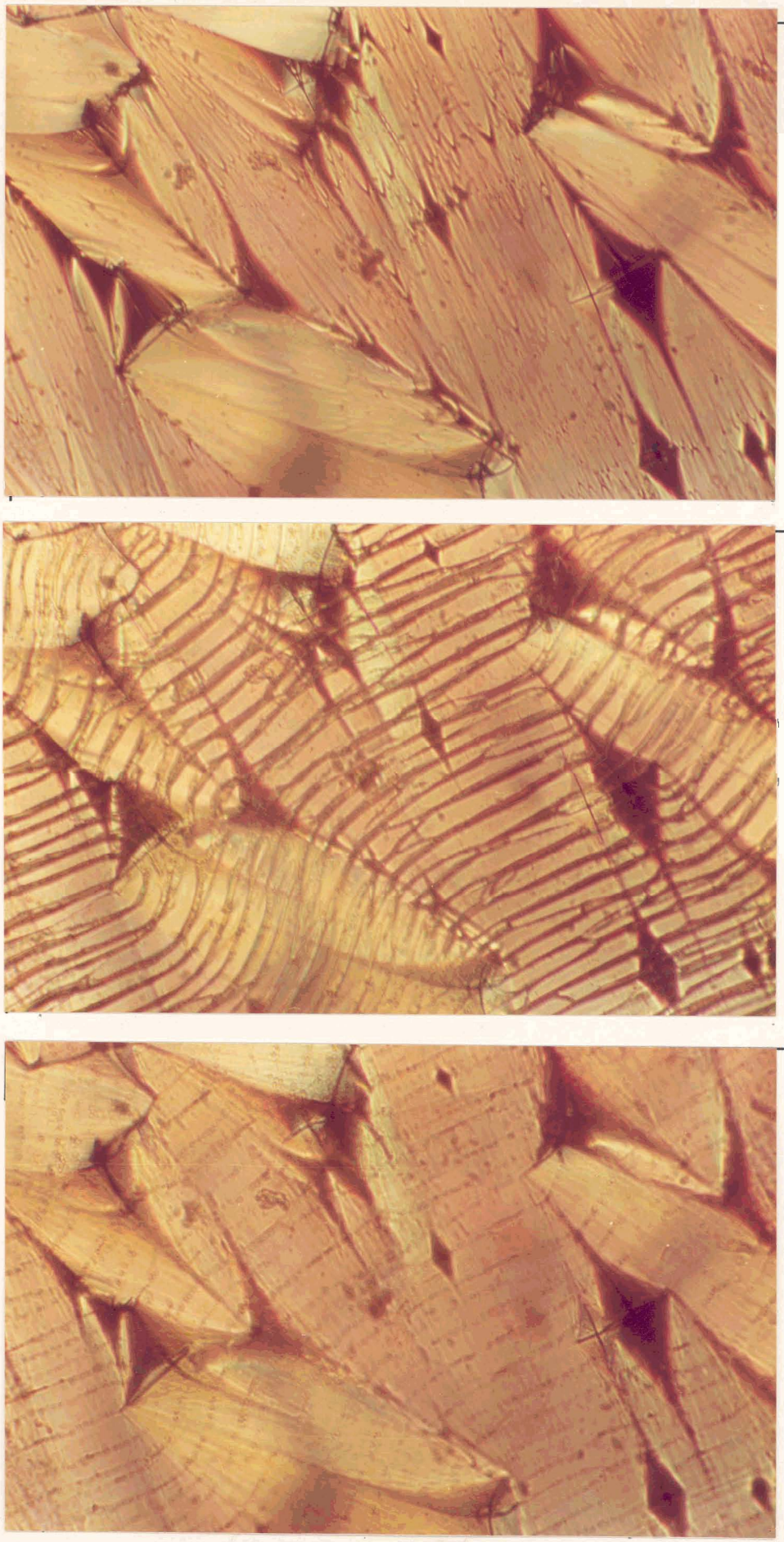

Figure 7.8: Microphotographs taken at 1.24 kbar showing ~ ~ t i ctextures of Sm A, Sm F and X phases.

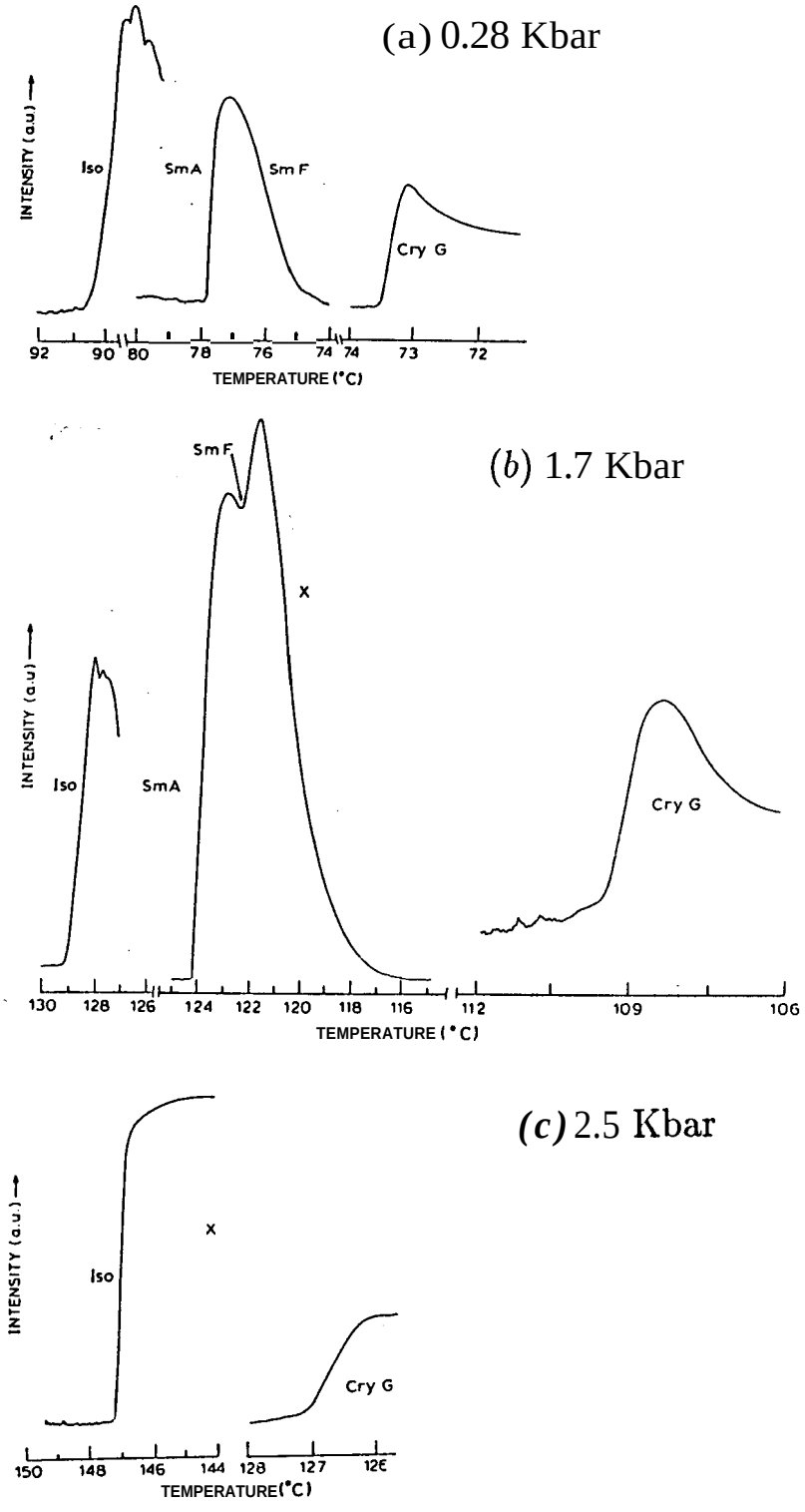

Figure 7.9: Raw scan showing thermal variation of intensity at 0.28 kbar, 1.7 kbar and at 2.5 kbar. Here Iso-refers to isotropic phase and X is the newly induced phase.

High pressure studies on fluid to hexatic transition

Table 1.4: $\left(\frac{dP}{dT}\right)$ values for 90.4.

	Transition	$\frac{dP}{dT}$ $bar/^oC$		
		at 1 bar	at Sm A-Sm F- X meeting point	at Iso-Sm A-X meeting point
1	Iso - Sm A	32	44.4	48
2	Sm A - Sm F	28.2	32.7	–
3	Sm F - X	–	27	32
4	X - Cry G	37.1	46	50

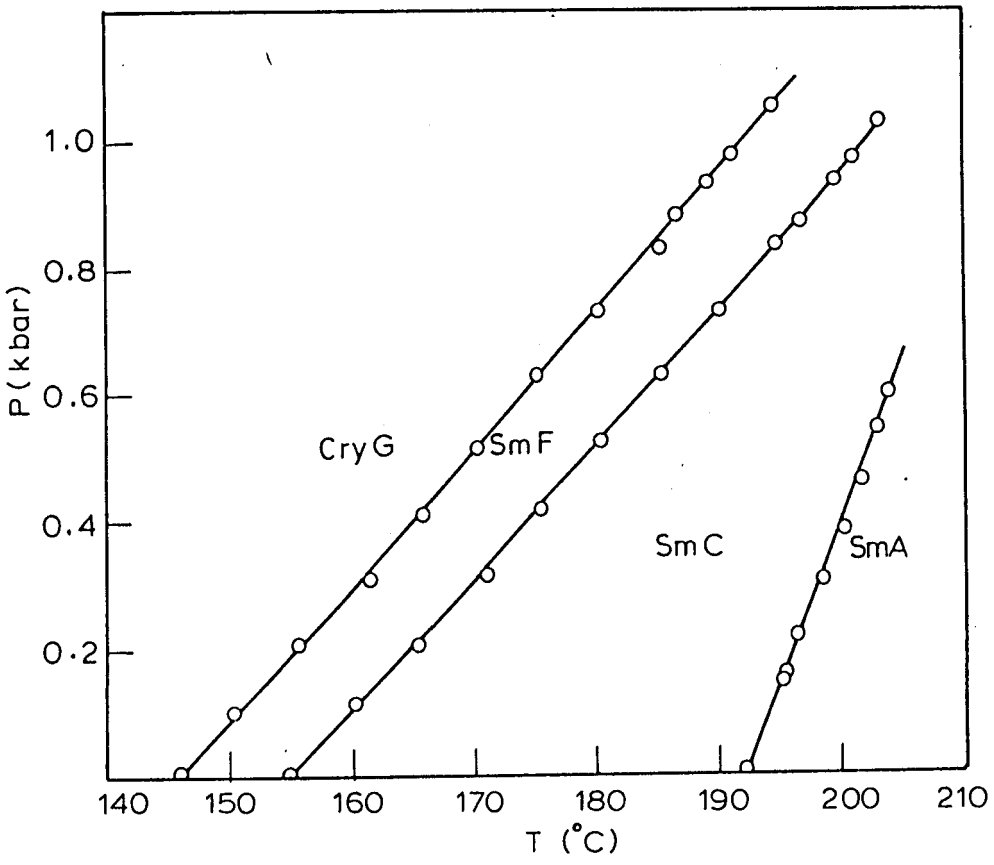

Figure 7.10: P-T diagram for TBOA. The destabilisation of Sm C phase appears to lead to Sm A-Sm C-Sm F meeting point at higher pressures.

Table 7.5: $\left(\frac{dP}{dT}\right)_{at\ 1\ \text{bar}}$ values for TBOA.

	Transition	$\frac{dP}{dT}$ bar / °C
1	Sm A - Sm C	**53.8**
2	Sm C - Sm F	20
3	Sm F - Cry G	20.6

Extrapolating the Sm A-Sm C and Sm C-Sm F boundaries to higher pressure, it appears that the three phases meet at ~1.3 kbar and at ~220°C. The Sm A-Sm C transition in this material is known to be second order[15] at 1 bar. Thus it would be interesting to see whether the nature of the Sm A-Sm C-Sm F meeting point is the same as obtained in the temperature-concentration diagram of 90.4 and TBBA, discussed in Chapter 2. Further, in view of the results obtained on 90.4 and 40.8 (Ref. 12), both of which posses a CH=N bridging group, it would be interesting to check whether the temperature range of the smectic A phase diminishes with increasing pressure in TBOA. It may be noted that due to the temperature limitation of our set up, we could not extend studies beyond 200°C.

For compounds (46OBC and 8SI*) with ester linkage group the stability of the Sm A phase increases with increase in pressure (Figures 7.5 & 7.6). In fact, Cladis et al[12,14,16,17] have argued that relative increase in the stability of Sm A phase with increase in pressure could be characteristic of ester compounds (possessing COO bridging groups) with symmetrically disposed chains. According to them this may be due to the strong short-range repulsive interactions of the lone pairs of electrons of the oxygen atoms of the ester and alkoxy functional groups. Our results also support this argument. In contrast it may be a general feature of compounds with Schiff base (CH=N) linkage group e.g., in 90.4, 5O.6[18] and 4O.8[12] that the Sm A phase is unstable at higher pressure.

Thus our results show that Sm A, orthogonal and tilted hexatic phases are likely to be more stable if the molecule has an ester linkage group as opposed to a Schiff base. However, many more studies are needed before one can generalise this behaviour.

References

[1] For a review on high pressure studies of liquid crystals till 1978, see S.Chandrasekhar and R.Shashidhar, Advances in liquid *crystals*,**4**, 83 (1979).

[2] S.Chandrasekhar, S.Ramaseshan, A.S.Reshamwala, B.K.Sadashiva, R.Shashidhar and V.Surendranath, Pramana, Suppl. **1**, 117 (1975).

[3] R.Shashidhar and S.Chandrasekhar, *J.Phys.*(Paris), 36, C1-49 (1975)

[4] P.E.Cladis, R.K.Bogardus, W.B.Daniels and G.N.Taylor, Phys.Rev.Lett., 39, 720 (1977).

[5] R.Shashidhar, Mol.*Cryst.*Liq.*Cryst.*, 43, 71 (1977).

[6] P.H.Keys, H.T.Weston and W.B.Daniels, Phys.Rev.Lett., 31, 628 (1973).

[7] S.M.Stishov, S.N.Nefedov and A.N.Zisman, JETP Lett., 36, 349 (1982); S.N.Nefedov, A.N.Zisman and S.M.Stishov, *Sov.Phys.JETP*, 59, 71 (1984); Geetha G. Nair, V.N.Raja, S.Krishna Prasad, S.Chandrasekhar and B.K.Sadashiva, Proceedings of *the XIII AIRAPT* International *Conference* on *High* Pressure Science and Technology, Bangalore, Ed. A.K.Singh (Oxford & IBI-I) New delhi, 1992 p 523.

[8] R.Shashidhar, B.R.Ratna and S.Krishna Prasad,*Phys.Rev.Lett.*,**53**, **2141 (1984).**

[9] R. Shasliidhar, A. N. Kalkura and S. Chandrasekhar, Mol. *Cryst.* Liq. *Cryst.* Lett., **82,311 (1982);** R. Shashidhar, S. Krishna Prasad and S. Chandrasekhar, Mol. *Cryst.* Liq. *Cryst.*, **103, 137 (1983).**

[10] R.Shashidhar, B.R.Ratna, V.Surendranath, V.N.Raja, S.Krishna Prasad and C.Nagabushan,*J.Physique Lett.*,**46**, **L-445 (1985);** V.N.Raja, B.R.Ratna, R.Shashidhar, G.Heppke, Ch.Bahr, J.F.Marko, J.O.Indeku and A.N.Berker,*Phys.Rev.***A** 39, **4341 (1989);** V.N.Raja,*Proceedings* of the *XIII AIRAPT International* Conference on High Pressure Science and Technology, Bangalore, Ed. A.K.Singh (Oxford & IBH) New delhi, **1992** p **514.**

[11] A.N.Kalkura, R.Shashidhar and N.Subramanya Raj Urs, **J.**Physique, **44**, **51 (1983);** S.Krishna Prasad, High Pressure Studies of Liquid Crystalline Transitions, Ph.D. Thesis, University of Mysore, **1985.**

[12] P.E.Cladis and J.W.Goodby, Mol.*Cryst.*Liq.*Cryst.*Lett., 72, **307 (1982).**

[13] A.N.Kalkura, R.Shashidhar, G.Venkatesh, D.Demus and W.Weissflog, Mol.*Cryst.*Liq.*Cryst.*, 84, **275 (1982).**

[14] P.E.Cladis and J.W.Goodby, *Mol.Cryst.*Liq.*Cryst.Lett.*, 72, **313 (1982).**

[15] S.Krishna Prasad, V.N.Raja, D.S Shankar Rao, Geetha G.Nair and M.E.Neubert, Phys.Rev. **A42, 2479 (1990).**

[16] P.E.Cladis, D.Guillon, J.Stamatoff, D.Aadsen, W.B.Daniels, M.E.Neubert and R.F.Griffith, Mol.*Cryst.*Liq.*Cryst.Lett.*, 49, 279 (1979).

[17] D.Guillon, J.Stamatoff and P.E.Cladis, J.Chem.Phys., 76, 2056 (1982).

[18] R. Shashidhar, A. N. Kalkura, and S. Chandrasekhar, Mol. Cyst. *Liq. Cryst.* Lett., 64, 101 (1980).